

## University of Groningen

### Protein biogenesis machinery is a driver of replicative aging in yeast

Janssens, Georges E.; Meinema, Anne C.; Gonzalez, Javier; Wolters, Justina; Schmidt, Alexander; Guryev, Victor; Bischoff, Rainer; Wit, Ernst; Veenhoff, Liesbeth M.; Heinemann, Matthias

Published in:  
eLife

DOI:  
[10.7554/eLife.08527](https://doi.org/10.7554/eLife.08527)

**IMPORTANT NOTE:** You are advised to consult the publisher's version (publisher's PDF) if you wish to cite from it. Please check the document version below.

*Document Version*  
Publisher's PDF, also known as Version of record

*Publication date:*  
2015

[Link to publication in University of Groningen/UMCG research database](#)

*Citation for published version (APA):*

Janssens, G. E., Meinema, A. C., Gonzalez, J., Wolters, J. C., Schmidt, A., Guryev, V., ... Heinemann, M. (2015). Protein biogenesis machinery is a driver of replicative aging in yeast. *eLife*, 2015(4), [e08527]. DOI: [10.7554/eLife.08527](https://doi.org/10.7554/eLife.08527)

**Copyright**

Other than for strictly personal use, it is not permitted to download or to forward/distribute the text or part of it without the consent of the author(s) and/or copyright holder(s), unless the work is under an open content license (like Creative Commons).

**Take-down policy**

If you believe that this document breaches copyright please contact us providing details, and we will remove access to the work immediately and investigate your claim.

*Downloaded from the University of Groningen/UMCG research database (Pure): <http://www.rug.nl/research/portal>. For technical reasons the number of authors shown on this cover page is limited to 10 maximum.*



## Influence of ZnO nanostructures in liquid crystal interfaces for bistable switching applications

Kaushik Pal<sup>a,1</sup>, Bihong Zhan<sup>a,1</sup>, M.L.N. Madhu Mohan<sup>b</sup>, Romana Schirhagl<sup>c</sup>, Guoping Wang<sup>a,\*</sup>

<sup>a</sup> School of Power and Mechanical Engineering, Wuhan University, 8 East Lake South Road, Wuhan 430072, China

<sup>b</sup> Liquid Crystal Research Laboratory (LCRL), Bannari Amman Institute of Technology, Sathyamangalam 638 401, India

<sup>c</sup> University Medical Center Groningen, Department of BioMedical Engineering, Ant. Deusinglaan 1, 9713 AV Groningen, The Netherlands



### ARTICLE INFO

#### Article history:

Received 18 August 2015

Received in revised form

22 September 2015

Accepted 27 September 2015

Available online 1 October 2015

#### Keywords:

ZnO nano structures

Hydrogen bonded liquid crystals

Electro-optical switching

### ABSTRACT

The controlled fabrication of nanometer-scale objects is without doubt one of the central issues in current science and technology. In this article, we exhibit a simple, one-step bench top synthesis of zinc oxide nano-tetrapods and nano-spheres which were tailored by the facial growth of nano-wires (diameter  $\approx 24$  nm; length  $\approx 118$  nm) and nano-cubes ( $\approx 395$  nm edge) to nano-sphere (diameter  $\approx 585$  nm) appeared. The possibilities of inexpensive, simple solvo-chemical synthesis of nanostructures were considered. In this article, a successful attempt has been made that ZnO nano-structures dispersed on well aligned hydrogen bonded liquid crystals (HBLC) comprising azelaic acid (AC) with p-n-alkyloxy benzoic acid (nBAO) by varying the respective alkyloxy carbon number ( $n=5$ ). The dispersion of nanomaterials with HBLC is an effective route to enhance the existing functionalities. A series of these composite materials were analyzed by polarizing optical microscope's electro-optical switching. An interesting feature of AC + nBAO is the induction of tilted smectic G phase with increasing carbon chain length. Phase diagrams of the above hybrid ZnO nanomaterial influenced LC complex and pure LC were constructed and compared. The switching times, the contrast ratio and spontaneous polarization of the nanostructures-HBLC composite film were carried out by systematic investigation. The sample preparation parameters, such as the curing time and curing intensity were optimized. The critical applied voltage to achieve the switching bi-stability of our device is only 4.5 V, which is approximately twice its threshold voltage for Freedericksz transition. This performance puts the hybrid structure at the top level in the state of the art in application oriented research in optics of liquid crystalline composite materials.

© 2015 Elsevier B.V. All rights reserved.

### 1. Introduction

Metal oxide nanostructures, including nano-rods, nano-wires and nanotubes, have attracted a great deal of interest because of their size-and morphology-dependent physicochemical properties and technological applications e.g. solar cells [1–3], electroluminescent devices [4], electro chromic windows [5,6] and chemical sensors [6–8] compared with their bulk phase counterparts [9,10]. To achieve high performance of these devices, the metal oxides were used in these applications are required to possess a high surface area as well as good electrical, electrochemical and structural

properties. ZnO is a direct wide band gap (3.3 eV) semiconductor with a large exciton binding energy of 60 meV at room temperature. Due to its wide applications in broad areas [11], much effort has been given to tailor the morphology and size during the past several years [11,12]. ZnO-based nanomaterials have received the most attention in many fields due to their superior properties in electro-optical bi-stable switching devices facilitated by their nano size. Several important synthetic parameters such as: precursor concentration, rate of evaporation and reaction time are found to determine the growth of ZnO nanostructures. These reaction parameters can be tailored and tuned amazingly to produce a rich variety of nanostructures ranging from nano-wire to nano-tetrapod and then nano-sphere. The fabrication strategy and high yield structured ZnO films can be achieved with an aqueous solution based route. This is a simple, low cost method which is compatible with industrial processing and fits with large scale production and is environmentally friendly. The controlled growth of the

\* Corresponding author.

E-mail addresses: [kaushikpal@whu.edu.cn](mailto:kaushikpal@whu.edu.cn) (K. Pal), [bihong\\_zhan@whu.edu.cn](mailto:bihong_zhan@whu.edu.cn) (B. Zhan), [guopingwang@whu.edu.cn](mailto:guopingwang@whu.edu.cn) (G. Wang).

<sup>1</sup> These authors contributed equally to this work.

inorganic structures driven by organic molecules through physical and chemical interactions represents an effective route to construct nanoscale materials with high surface to volume ratio. The complex agents such as cetyltrimethylammonium bromide (CTAB) have been used to control the variety growth of ZnO morphology.

Liquid crystal (LC) produces a rich variety of complex, controlled and ordered a three-dimension structures of constituent anisotropic molecules which can be varied by external fields, boundary conditions, embedded particles, light, temperature changes, and other relatively weak external stimuli [13,14]. Hydrogen bonded LC complexes (HBLC) have attracted a great deal of interest, due to their structural and dynamic properties as they play significant roles in many chemical, physical and display technology systems [15,16]. By choosing an appropriate proton acceptor and proton donor, stable intermolecular hydrogen bonds can be formed and thereby they provide a novel system with new properties [17,18]. In such LC compounds, the effect of hydrogen bonding is very important for the material properties. LC materials are generated by inter-molecular hydrogen bonds which have been studied and investigated extensively to design novel LC materials [19–22]. The recent progress in forming uniform dispersions of HBLC in various types of metal oxide (ZnO) nanostructures opens a new set of possibilities in engineering material composites with novel material behavior. Since the discovery of bi-stable switching in a surface stabilized ferroelectric liquid crystals first employed by Clark and Lager wall [23]. The unusual optical features of LC make them indispensable in many modern technologies, including displays and optoelectronics. Further improvement and fine tuning of the electro-optic (EO) properties of LC are subject to intense research for which blending nanomaterials with HBLC have been proved to be the most effective non-synthetic way.

During the last decade, nano dispersions in ferro-electric or anti-ferroelectric liquid crystals are more extensively studied than HBLC. Numerous efforts have been employed to change the EO properties of the ferroelectric/anti-ferroelectric liquid crystals doping with nanomaterials [24], but the use of non-covalent interactions have great potential in the design of functional organic liquid-crystalline materials. For molecular aggregation, hydrogen bonding plays an important role in the association of molecules. In LC, mesomorphism results from the proper combination of molecular interactions and the shape of molecules. Dipole–dipole interaction has long been taken into consideration in the design of liquid-crystalline molecules. Due to the demand for a wide variety of electro-optic materials with properties suitable for the display applications [25–28], research activity has grown in this area. Although the first reports of HBLC date back to the 1960s [29,30], much research have taken place in the last two decades [31–34]. It is noticed that in HBLC lower bonding and activation energies showed a profound influence on their thermal properties, viz. clearing points, enthalpies, and mesomorphic phase behaviors. Hydrogen bonding is a powerful tool for assembling molecules for noncovalent interactions in nature. The main advantage of hydrogen-bonded mesogens is that their LC properties can be tuned easily by changing the H-bond donor=acceptor or percentage of molar composition. Stable and dynamic molecular complexes can be prepared by simple molecular self-assembly processes using such hydrogen bonding. A number of such liquid crystal systems have been investigated following the reports of Kato et al. [32–37], which indicates that the mesomorphism results from a proper combination of molecular interactions and shapes of the molecules. There has been an increasing development of computational chemistry in the past decade. Many imperative chemicals and physical properties of biological systems can be predicted by various computational techniques [38,39]. In recent years, density functional theory (DFT) with a better exchange-correlation functional has

made it possible to calculate many molecular properties with comparable accuracies to traditional correlated ab initio methods [40]. Literature survey also reveals that the DFT has a greater accuracy in reproducing the experimental results [41–45]. However, self-assembly in living nematic [46,47] which are essentially low-molecular-weight LC has also been reported. The mechanism of hydrogen bonding for the case of self-assembling systems formed by polymer liquid crystal and extended chain polymer liquid crystal has been extensively studied [48]. One of the key breakthroughs in recent research activities that have focused on the systematic study of ZnO nanomaterials dispersed double HBLC possessing a mesogenic ligand (*n*-*p* alkyloxy benzoic acids, *n*BOA) and azelaic acid (AC). Moreover, polarizing optical microscopy revealed various phases in different textural appearance proof the influence of the nanomaterial. This approach mainly informative electro-optical switching behavior of twist nematic phase. A range of remarkable characteristics is then presented, organized into sections describing the optical, electrical and electro-optical phase transition and DC bi-stable switching properties. Indeed, the unique mechanism of the other display parameters such as: spontaneous polarization, rotational viscosity, dielectric constants, switching response techniques is also investigated in these nanostructures-HBLC composite and found quite convincing to the described observations in this article, which is consistent with experimental findings, providing insights into the nature of the studied soft matter composites.

## 2. Materials and experimental

### 2.1. Materials

Starting materials were used in this investigation were analytical grade, commercially available and received without further purification. Zinc nitrate  $[Zn(NO_3)_2 \cdot 5H_2O]$ , ammonium hydroxide  $[NH_4OH]$ , cetyltrimethylammonium bromide [CTAB], and hydrazine monohydrate (80% v/v) were used as starting ingredients for synthesis of various types of nano structured molecules. Hydrogen bonded liquid crystals is composed of *p*-*n*-alkyloxy benzoic acids *n*BAO with azelaic acid supplied by Sigma–Aldrich (Germany). N,N-dimethyl formamide (DMF) and other solvents were purchased in High Performance Liquid Chromatography (HPLC) grade and used as received.

### 2.2. Synthesis

In our typical synthesis zinc oxide nano-wire, nano-tetrapod and nano-sphere were grown in a furnace with two heating zones by simple solvo-chemical track. As source material, an equimolar mixture of high purity ZnO salt (Sigma–Aldrich 99.99%) and reducing agent (hydrazine monohydrate) was placed in a beaker located in heating zone I held at 85 °C and vigorously stirred for around 50 min. A portion of the ZnO aqueous solution was separated in another glass container before adding reducing agent and stored for our last set of experiment. The rest of the solution the surfactant CTAB (0.055 mmol) was added drop wise followed by adding 0.55 mol concentration of  $NH_4OH$  solution. The resulting mixture was left to vigorous stir at 70 °C for 3 h to complete the whole reaction mechanism. We investigated that in our first set of experiment white precipitate was obtained, while next gray colored precipitate was produced during the addition of ammonia solution. Both solutions were filtrated and washed with the flow of 1 liter double distilled water and ethanol several times. Desired samples were dried under a continuous flow of clean  $N_2$ . The resulting white powder samples were finally collected in two separate containers for further spectroscopic investigation.

In a different set of experiments 0.055% of ZnO nanomaterials were blended with typical concentrations of two moles of 5BAO's

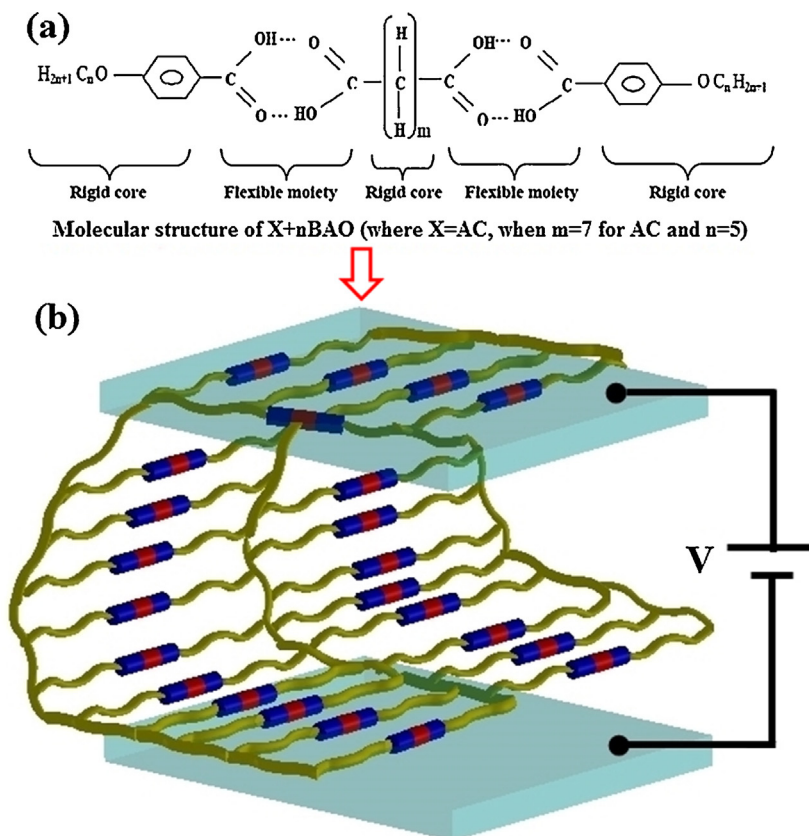


**Fig. 1.** (a) Chemical formula of hydrogen bonded liquid crystal components (azelaic acid with p-n-alkoxy benzoic acids) and (b) orientation of liquid crystals confined geometry sandwiched ITO cells.

with one mole of azelaic acid in DMF and left under continuous stirring until the solvent evaporated and again crystallized with dimethyl sulfoxide (DMSO) and the yield varied from 75% to 99%. The formation of multimer is avoided by recrystallization of the product. Suspensions fabricated in this way were then put into photorefractive LC cells. The molecular structures of the present homologous series as depicted in Fig. 1, where  $n$  represents the alkoxy carbon number ( $n=5$ ) and  $m$  is the number of H-C-H spacer groups, here  $m=7$ .

### 2.3. Characterizations

The morphologies of the ZnO nano-structures were grown on  $\text{SiO}_2$  substrates and characterized by field emission scanning electron microscopy (Model: SIGMA ZEISS FE-SEM) using a JEOL electron microscope 6700 equipped with a field emission gun operating at 3 kV. The detection of chemical composition by energy dispersion spectroscopy (Model: EDAX GENESIS, 200 V–30 kV, AMETEK, USA). To evaluate the morphology of ZnO thin film cross-sectional images of the samples were precisely observed using a Transmission Electron Microscopy system (TEM) JEOL JEM-2100 (HR) equipped with an EDX device (GENESIS XM2). The TEM samples were sliced to a thickness of tens of nm perpendicularly to the carbon coated copper grid at an acceleration voltage of 200 kV. Moreover, SAED patterns and high-angle annular dark field scanning TEM (ORIUS™ SC 1000 CCD) images were also obtained for crystalline analysis and Z-contrast imaging. AFM grain analysis was performed with high scanning rate ICCD camera (Roper Scientific). The surface morphology and conducting mode AFM surface current were measured by Multimode8, Bruker. The frequency dispersion dielectric data were recorded at room temperature at frequencies ranging from 10 Hz to 20 MHz using low

frequency Impedance Analyzer Spectroscopy (Model: Microtest-6620). The DC conductivity of bi-stable switching  $I$ - $V$  response measurement with a digital source meter (Model: Agilent 33522A, 30 MHz function/Arbitrary waveform generator).

The commercial electro-optical LC cells with ITO electrodes (electrode area  $4\text{ mm} \times 4\text{ mm}$ ) and alignment layers were deposited on the inner surface of the confining substrates; the alignment layers were rubbed in unidirectional and assembled in an antiparallel fashion with respect to the rubbing directions for a planar alignment. The cell gap was maintained with  $2\text{ }\mu\text{m}$  spacer placed between the substrates. The smectic helix was reoriented parallel to the substrates by cooling the material from isotropic ( $109.1^\circ\text{C}$ ) to room temperature with or without a voltage of  $5\text{ V } \mu\text{m}^{-1}$  at 1 kHz. Surface stabilized smectic uniform lying helical texture and electro-optical switching with different temperature variation calculated by polarizing optical microscopy (Model: OLYMPUS, CX31, 6J09934 Japan) with a signal generator (Model: U8031A). The spontaneous polarization ( $P_s$ ) and the relaxation time were measured by using a polarization reversal method Eq. (1) and calculated with the help of the following relation [24,49,50]:

$$P_s = \left( \frac{1}{2A} \right) \int i(t) dt \quad (1)$$

All associated measurements were based on graphical computation, which follows Eq. (2). The viscosity ( $\gamma$ ) was determined from the measured value of the polarization ( $P_s$ ) and the switching time ( $\tau$ ) using the following relation [24]:

$$\tau = \frac{\gamma}{1.75 P_s E} \quad (2)$$

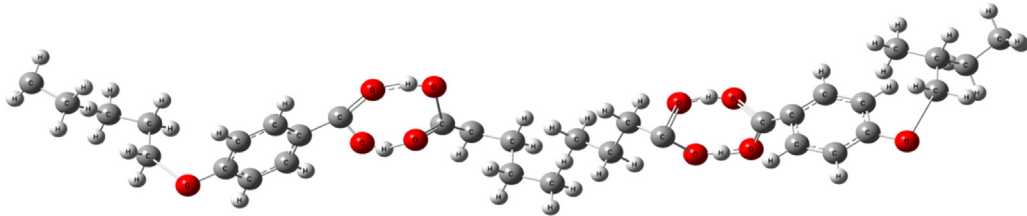


**Fig. 2.** Simulated molecular dynamics of HBLC (AC + 5BAO) geometric structure and atomic numbering scheme of all the hydrogen bonded mesogens.

'Smectic G' phase appeared by evacuating the LC using the appropriate solvent. The appropriate phase sequence of pure LC was shown below:

(Cr 91.3 °C ↔ Sm G 94.5 °C ↔ N 97.3 °C ↔ TN 100.2 °C ↔ Iso 109.1 °C).

#### 2.4. Computational details

Density functional theory computations have been performed using Gaussian 03W program package [51] with Becke-3-Lee-Yang-Parr hybrid exchange-correlation three-parameter functional (B3LYP) [52,53] level with standard 6-311G (d, p) basis set. The geometry optimization has been performed [54] using the same level of theory and the frequencies were calculated to check the presence of any imaginary frequency and to evaluate the zero point corrections. In all the computations unrestricted open-shell approach was adopted. Unrestricted open-shell approach can offer accuracy approaching through the molecular modeling and simulation methods are increasingly at the forefront of elucidating mechanisms of liquid crystals reactions, and shedding light on the determinants of specificity and efficiency of liquid crystal compounds. Modeling protocols commonly applied in studying liquid crystal reactions are outlined here, and some practical implications are considered, with nanomaterials used as a specific example. Also molecular mechanics (MM) methods are important in simulations of liquid crystals, even though typical MM methods cannot model chemical reactions. So we are using molecular dynamics simulations, or combined with quantum mechanical methods in QM/MM calculations on reactions. This is important because a simple functional form typically we are using in MM energy functions (force fields), e.g. harmonic terms represent the energy of bond stretching and valence angle bending, Van der Waals interactions and simple periodic terms describe torsional angles. The unrestricted open-shell majority of these considerations only apply to large, entire (or truncated) liquid crystal model for MM or QM/MM simulations. The interaction energy during mesogen formation through the hydrogen bonded interface was calculated by super molecule method [55,56]. The interaction energy was calculated using Eq. (3).

$$\Delta E = E(A_1, A_2, A_3, \dots, A_N) - \sum_{i=1}^N A_i \quad (3)$$

where  $E(A_1, A_2, A_3, \dots, A_N)$  are the energies of the isolated monomers.

The natural bonding orbital (NBO) calculations [57] have been performed using NBO 3.1 program (Gaussian 03 package). The intermolecular delocalization or hyper conjugation leads to various second order interactions between the filled orbitals of one subsystem and the vacant orbitals of another subsystem. The hyper conjugative interaction energy was inferred from the second-order perturbation approach  $E(2)$  as follows [58] (Eq. (4)):

$$E(2) = -\eta_\sigma \frac{\langle \sigma | F | \sigma \rangle^2}{\varepsilon_{\sigma^*} - \varepsilon_\sigma} \quad (4)$$

where  $\sigma | F | \sigma^2$  and  $F_{ij}^2$  is the Fock matrix element between  $i$  and  $j$  is NBO orbitals,  $\varepsilon_{\sigma^*}$  and  $\varepsilon_\sigma$  are the energies of  $\sigma$  and  $\sigma^*$  NBO's, and  $n_\sigma$  is the population of the donor  $\sigma$  orbital. The formation of intermolecular hydrogen bonds diagram in (AC + 5BAO) and simulated geometric analysis as shown in Fig. 2. The hydrogen bond interactions among  $O_{16} \cdots H_{22} - O_{21}$ ,  $O_{17} - H_{18} \cdots O_{20}$ ,  $O_{43} - H_{44} \cdots O_{58}$ ,  $O_{42} \cdots H_{57} - O_{59}$  groups have been observed. The intermolecular hydrogen bonds are found to be linear and the bond lengths are 1.652, 1.673, 1.651 and 1.674 for  $O_{16} \cdots H_{22}$ ,  $H_{18} \cdots O_{20}$ ,  $O_{58} \cdots H_{44}$  and  $H_{57} \cdots O_{42}$  respectively. This clearly revealed the double hydrogen bond formation of the 5OBA mesogen.

Moreover, the frequency dispersion dielectric data were recorded at room temperature in the frequency range from 10 Hz to 20 MHz using Impedance Analyzer on a 1 μm thick sample cell. The test cells for dynamic measurement were prepared using 0.7 mm ITO-coated polished glass plates having 16 (4 mm × 4 mm) pixels imprinted on the ITO coating by photolithography. The thickness of the cells was about 0.1 μm, thin enough to allow surface stabilization of the specimen. Frequency dependent complex dielectric permittivity  $\varepsilon^*(\omega)$  is determined using the following equation [59,60]:

$$\varepsilon^*(\omega) = \frac{1}{j\omega C_0 Z^*(\omega)} = \frac{C_p}{C_0} - j \frac{1}{\omega C_0 R_p} = \varepsilon' - i\varepsilon'' \quad (5)$$

where  $\varepsilon'$  is the dielectric constant and  $\varepsilon''$  is the dielectric loss. This frequency dispersion dielectric data were recorded within the room temperature in the frequency range from 10 Hz to 13 MHz using a HP4192 Impedance Analyzer on a 1 μm thick sample cell. Where  $j$  denotes the square root of  $-1$ ,  $\omega (=2\pi f)$  is the angular frequency,  $Z$  stands for the complex impedance,  $C_0$  and  $C_p$  is the capacitances of the cell under the vacuum and that filled with a dielectric bulk, respectively,  $R_p$  is the effective parallel resistance of the dielectric cell (consisting of a planar LC bulk of this study), and  $\varepsilon'$  and  $\varepsilon''$  represent the real and imaginary parts of the complex dielectric constant, respectively. Detailed investigation of sample preparation and distribution into ITO cells and confined geometry can be represented in Fig. 3.

## 3. Results and discussions

### 3.1. Morphology analysis of field emission scanning electron microscopy (FE-SEM)

The morphology and the orientation of ZnO nanostructures grown onto acetone vapor cleaned Si wafer were studied by FE-SEM in Fig. 4a. The large amount of distributions of hexagonal nano-wires were grown preferentially average uniform diameter ≈ 24 nm and length ≈ 118 nm. Those nano-wires were featured by a narrow size distribution. Certain application of ultrasonic vibration to those nano-wires becomes centered together deformed nano-tetrapod structures magnifying image as shown in Fig. 4b. The next set of solvo-thermal attempt led to uniform nano-cube structure as shown in Fig. 5a. We additionally feed the precursor by the typical concentration of cationic surfactant (CTAB) and NH<sub>4</sub>OH, which reacts upon heating to yield novel nano-sphere

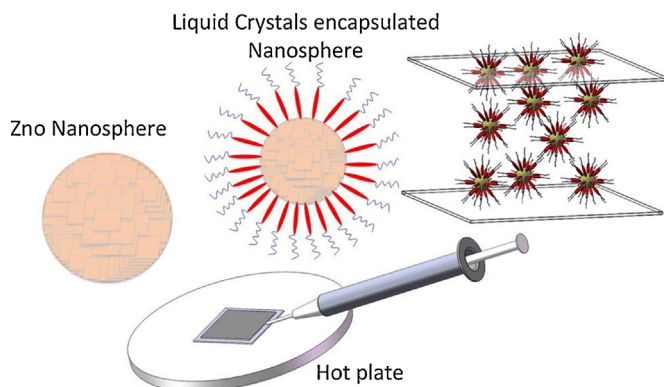


**Fig. 3.** Schematic representation of ZnO nano-sphere composed of nano-cubes, those embedded with liquid crystals confined into ITO sandwiched cell and sample dispersion through capillary action by syringe.

structures. A closer observation shows the broadening of the edge distribution and an increasing proportion of interconnected nano-cubes form nano-sphere with diameter  $\approx 585$  nm, which is composed by nano-cubes of edge  $\approx 395$  nm, in Fig. 5b. Additionally, Fig. 5c presents a diagram of the evolving warm like morphologies of updoped HBLG FE-SEM image under dispersion of a solvent. While, ZnO nano-structures start nucleation on the dispersion of HBLG, which was fully capped as depicted in Fig. 5d.

### 3.2. Structural analysis by high resolution transmission electron microscopy (HR-TEM)

More details on morphological and structural features are given in Fig. 6 using HR-TEM for nano-cubes based nano-spheres. Individual micro-spheres grown from the film were collected by scratching sample dissolved into ethanol solution and uniformly distributed. The nano-sphere was submerged by LC clearly shown in FE-SEM, Fig. 5d. A close observation of a typical TEM image (Fig. 6a) shows that both extremities of the nano-spheres were different.

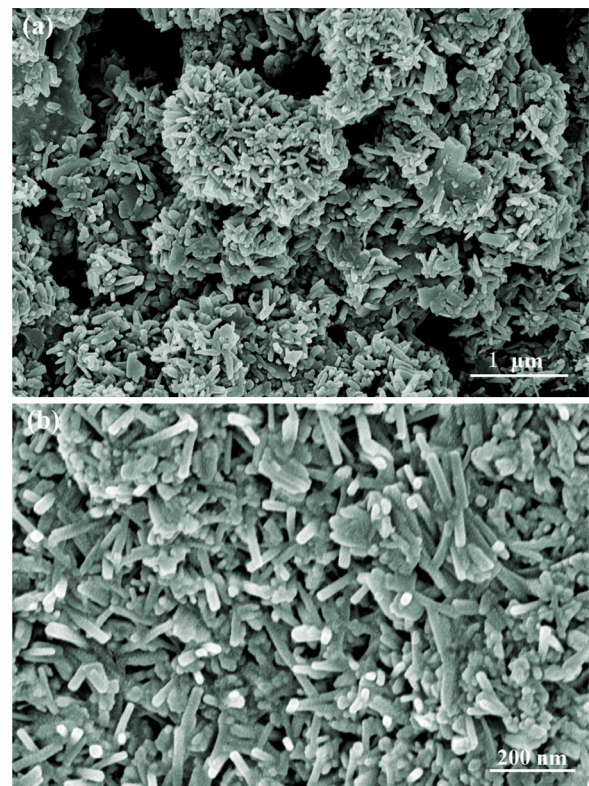


**Fig. 4.** FE-SEM images of uniform ZnO (a) nano-wires, high magnification (2 diameter  $\approx 24$  nm and length  $\approx 118$  nm), (b) ultrasonic vibration nano-tetrapods structures obtained at low magnification (1  $\mu$ m) by assistance of reducing agent (hydrazine monohydrate), in Solvo-chemical process.

Arrows indicate the roughened extremities that are attached to ZnO nanocrystal seeds (Fig. 6b). The other rounded extremities correspond to those that were exposed to the reaction medium. Selected area electron diffraction (SAED) patterns shows spots (Fig. 6c),

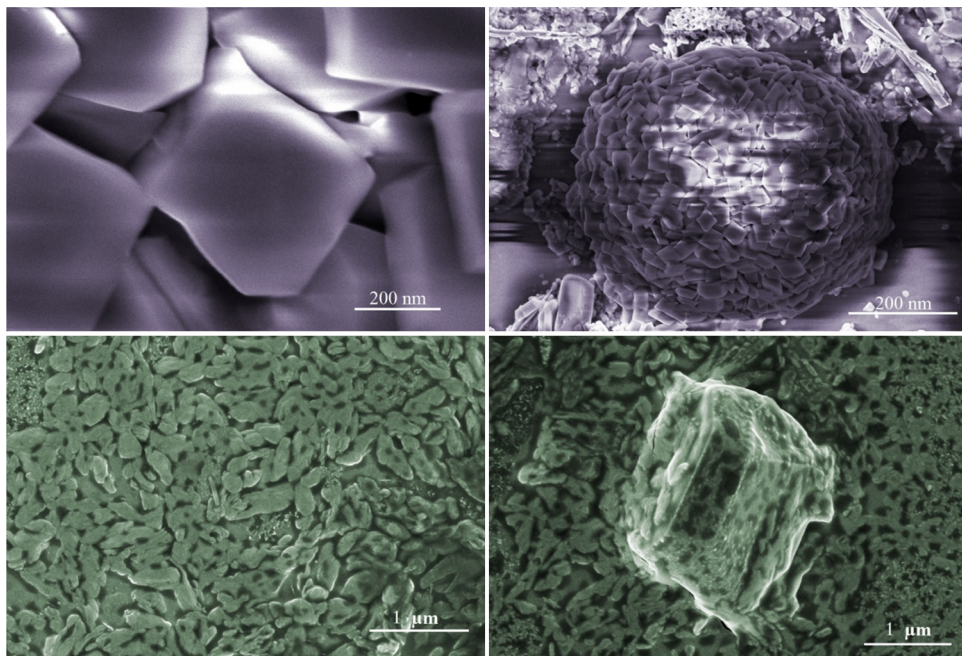


**Fig. 5.** FE-SEM images illustrating the growth of uniform (a) nano-cubes obtained by adding surfactant CTAB in high magnification (edge  $\approx 395$  nm), (b) nano-sphere is obtained by solvo-thermal process in low magnification (diameter  $\approx 585$  nm), (c) warm like hydrogen bonded liquid crystals (azelaic acid with p-n-alkoxy benzoic acids) thin film, and (d) nano-sphere dispersion with liquid crystal.

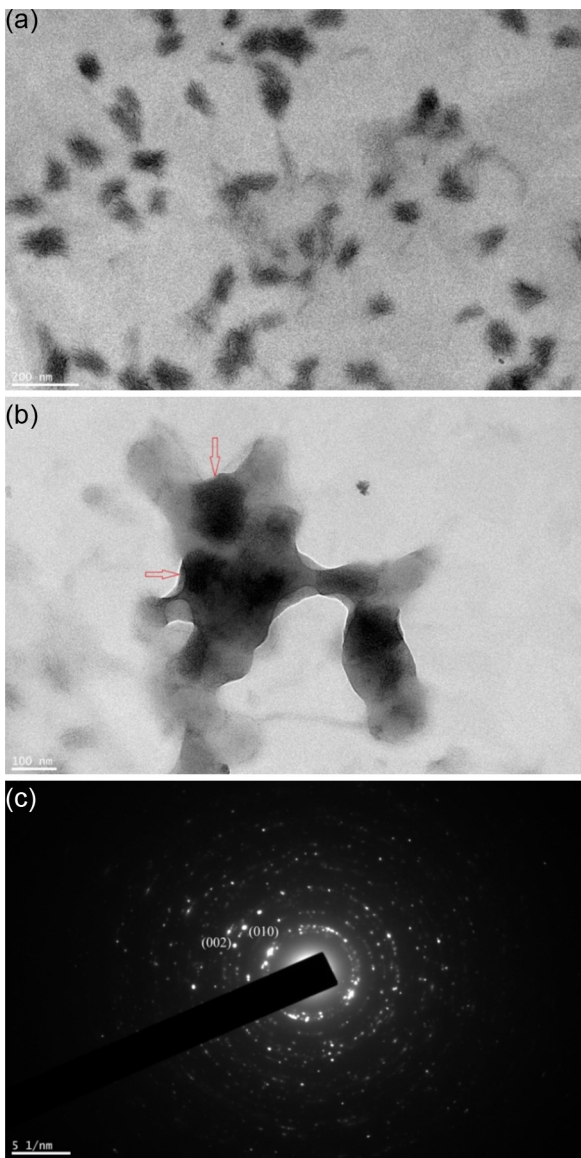


**Fig. 6.** Typical high resolution TEM image of the as-prepared: (a) ZnO nano-spheres thin film, (b) nano-sphere dispersed on liquid crystals, and (c) nano-sphere under liquid crystalline materials SEAD pattern.

which can be indexed to the crystallographic planes of the ZnO nanostructures. Moreover, the zone axis deduced from this picture correspond to the (010) plane, which is associated with the lateral side of the nano-spheres. These results confirmed that nano-sphere fully encapsulated by LC materials were poly crystalline in nature with specific orientations along the *c* axis. As it was already noticed, the nature of the reducing agent (hydrazine monohydrate) and surfactant (CTAB) helps to control the morphology and the ZnO nanostructures as well as smooth dispersion under liquid crystal interfaces [61–63].

### 3.3. Energy dispersion spectroscopy (EDS)

The typical pattern of Energy Dispersion Spectroscopy (EDS) performed in thin film dispersion of silicon wafer substrate as shown in Fig. 7, implies an atomic ratio of zinc and oxide of 26.3–53.1 for nano-wire. This pattern verifies the high purity of as-prepared ZnO nano materials were used in this experiment.

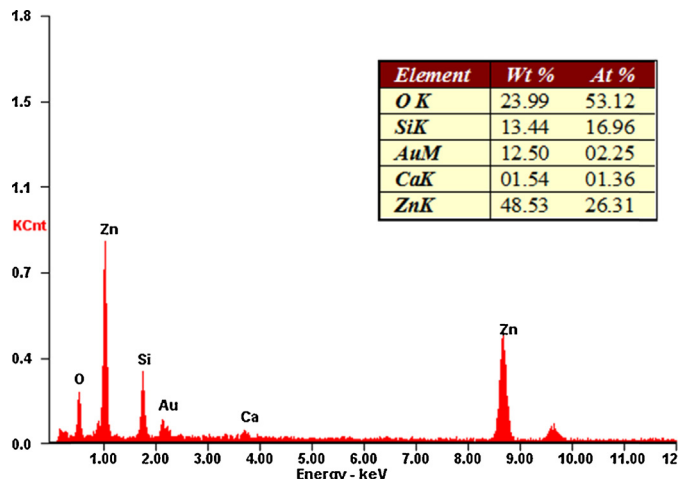


**Fig. 7.** Distribution of chemical composition of EDS profiles corresponds to ZnO nano-sphere as prepared by solvo-thermal assisted process in thin film distribution on silicon wafer substrate.

### 3.4. Surface morphology and current analysis by atomic force microscopy (AFM)

Reliable and understandable surface topography, surface roughness, surface current e.g., Electrical measurements through the CP-AFM setup requires a well-characterized conductive tip. The AFM in Fig. 8a shows the topography for the ZnO nano-rods were well dispersed in a smooth cover slip glass surface and the average surface roughness (RMS) value is about 3.1 nm and thickness of thin film around 425 nm with the scanning area of 2.0  $\mu\text{m} \times 2.0 \mu\text{m}$ . Depending on the experimental conditions, the AFM conductive tip should be the most suitable in terms of serial resistance that must be taken into account in the electrical analysis of nano-wire. The CP-AFM more specifies the sample configuration and biasing were displayed in Fig. 8b. In case of horizontal nano-wire, the DC bias voltage was applied to the sample placed on copper pad, while maximum 373 pA current flow through the surface. The Fig. 8c yields electrical conductivity when the rods were not broken or disconnected from the Cu pad. In order to get more precise information about the variation of the local resistance to function of the applied bias, CP-AFM were locally used for investigating the *I*–*V* characteristics on individual ZnO nano-wire. Fig. 8c displays one identifiable slope fitted (red line) by exponential growth passing through the origin. Indeed, the analysis of the negative current increases exponentially with applied voltage and some noise current also appeared due to surface roughness.

### 3.5. Electro-optical switching response by polarizing optical microscopy (POM)

So far, the experimental characterizations have been carried out in thin sandwich cells [35], where the mesogens can be aligned by surface treatment and the layers may be oriented by some shearing techniques. Electric fields can be applied by means of transparent electrodes at the glass plates. While this geometry may be important from the application aspect, it poses some problems during preparation; in particular, the layer alignment is not easily achieved. Moreover, the evaluation of electro-optical data is quite complex because of the influence of cell boundaries. Surface stabilized switching response by POM is the most significant instrument for cell structures and dynamics. The thickness of such films can vary from thousands down to two layers. One can often treat these systems as quasi-two-dimensional, with a large experimental accessible planar area. The orientation and dynamics of the

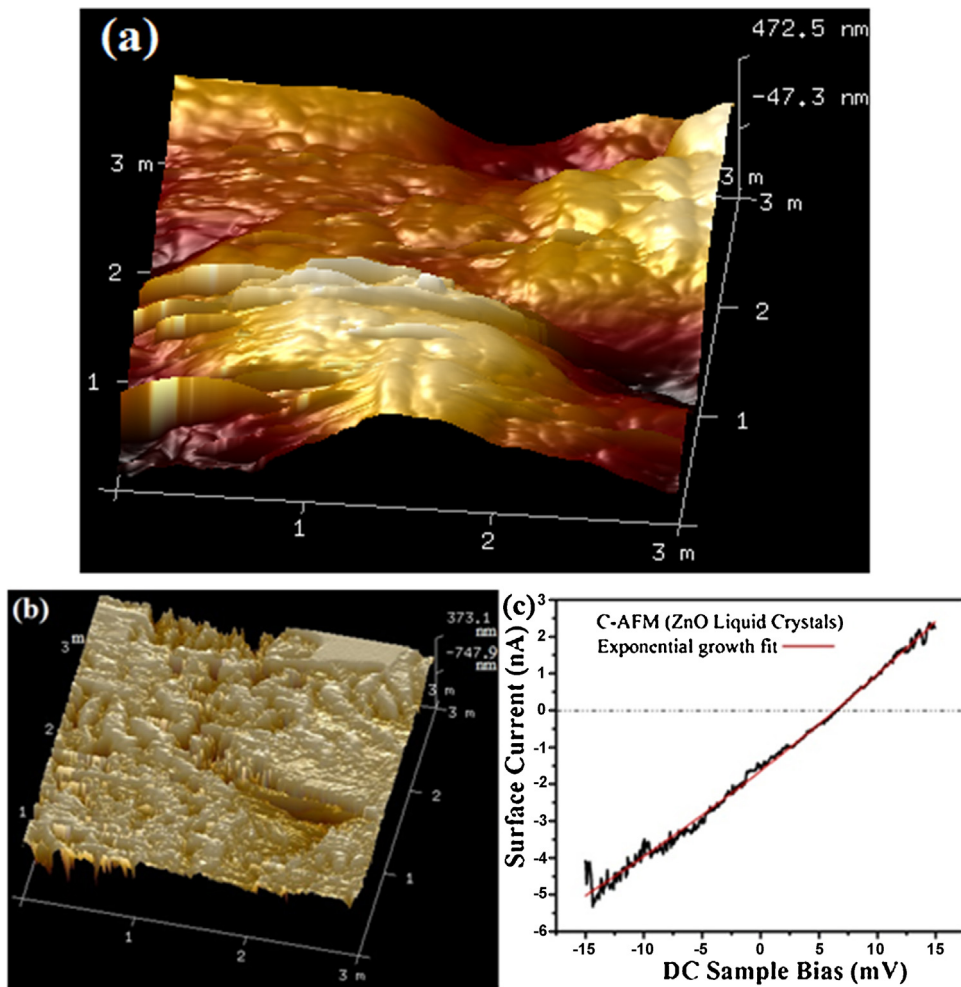


**Fig. 8.** (a) Thin film surface morphology study through atomic force microscopy (AFM) topography for the ZnO nano-wires in non-contact mode, (b) a contact mode (C-AFM) of ZnO nanomaterials dispersed on liquid crystal morphology of the surface when the current passing through it, and (c) surface current profile with applied DC sample bias field.

LC director can be observed in samples with microscopically well ordered layers.

### 3.6. Electro-optical switching texture studies

Our sample consists of a commercial room-temperature smectic mixture, whose dielectric anisotropy and electro-optical (EO) switching changes at a specific inversion frequency. Fig. 9 shows the POM textures of short pitched liquid crystal (pure) with temperature variation. The LC material is heated then cooled slowly to room temperature under an electric field. Uniform textures were slowly developed as the temperature is cooled to room temperature. A small bias field is maintained to prevent cells for electro-optical switching. The phase diagram for pure AC+nOBA homologous series (azelaic acid with p-n-alkoxybenzoic acid complexes) is composed of three different phases e.g. smectic G, nematic and twist Nematic.

A texture study through POM analysis ensures from Fig. 9a, liquid crystal first heated until reaching in its isotropic temperature ( $109.1^{\circ}\text{C}$ ) and cooled down slowly. This parallel and antiparallel cross alignment of LC molecules whose optical axis is laid at  $30^{\circ}$  with respect to the crossed polarizers. The isotropic liquid placed between glass slides was examined through a slow cooling rate of  $5^{\circ}\text{C min}^{-1}$  with applied bias voltage 5 V to the cell.

Marbled patterns, even at lower temperature resulted in Fig. 9b. This image can be regarded at temperature  $94.5^{\circ}\text{C}$  due smectic G phase. Gradual increase of temperature earlier marble pattern changed, while a free standing marble pattern appeared at temperature  $97.3^{\circ}\text{C}$  (Fig. 9c) corresponding nematic phase. There is a small heat transition occurring during phase change between nematic to twist nematic rainbow color shiny droplet (Fig. 9d). However, ZnO nano-sphere encapsulated liquid crystal electro-optical switching texture was studied with little different temperature transition comparable to pure LC phase transitions as shown in Fig. 10a directed porous texture identified to the surface. Bright field droplet design marble pattern of smectic G phase obtained at temperature  $95^{\circ}\text{C}$  as shown in Fig. 10b. Small heat increase to the cell nematic phase of a continuous pattern free standing film was obtained at temperature  $97.6^{\circ}\text{C}$  located normal to the surface, resulted in Fig. 10c. While a twist nematic oily droplet texture appeared at temperature  $100.8^{\circ}\text{C}$  corresponding to Fig. 10d. The corresponding phase sequence of ZnO nanostructures influenced by LC is given by; (Cr  $90.5^{\circ}$   $\leftrightarrow$  Sm G  $94^{\circ}$   $\leftrightarrow$  N  $97^{\circ}$   $\leftrightarrow$  TN  $100^{\circ}$   $\leftrightarrow$  Iso  $108.5^{\circ}$ ).

The dependence of electrical and optical response time ( $\tau$ ) on temperature in the Smectic phase of the liquid crystal and ZnO nanomaterials dispersed HBL, as shown in Fig. 11a and b. It has been observed that smectic LC having been doped with ZnO shows almost 20% faster response compared to pure HBL sample at  $30^{\circ}\text{C}$ .

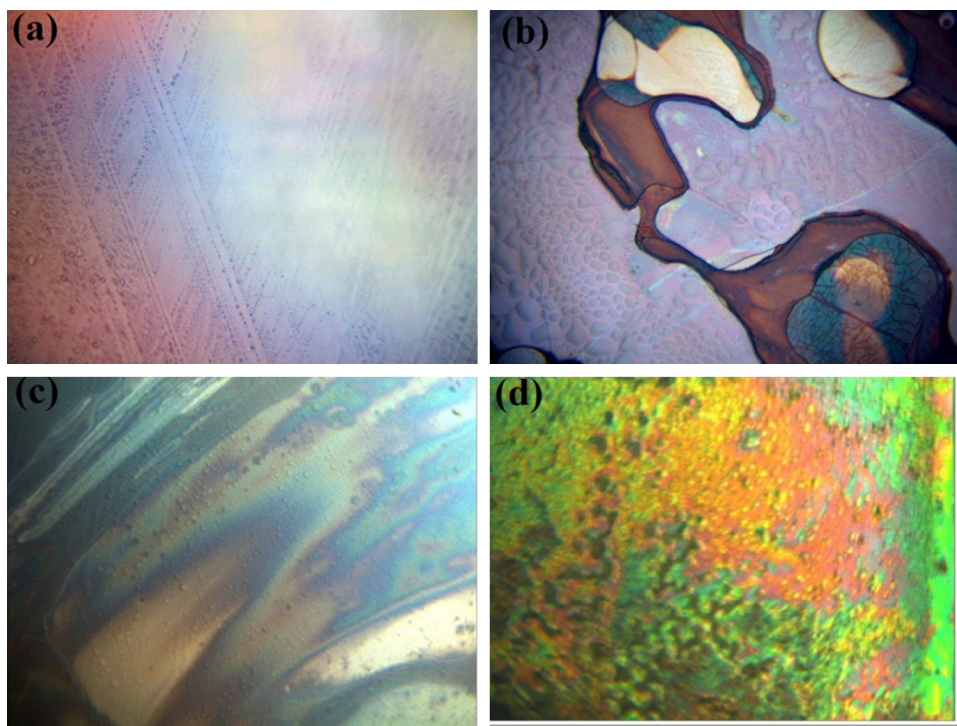


**Fig. 9.** A collection of texture studies optical micrograph of pure liquid crystal (AC + 5BAO): (a) cross parallel and anti-parallel to the plane of crystals phase at temperature 91.3 °C, (b) smectic G phase droplet texture appeared at temperature at 94.5 °C, (c) nematic (N) phase marble pattern at temperature 97.3 °C, and (d) twist nematic oily droplet pattern at temperature 100.2 °C.

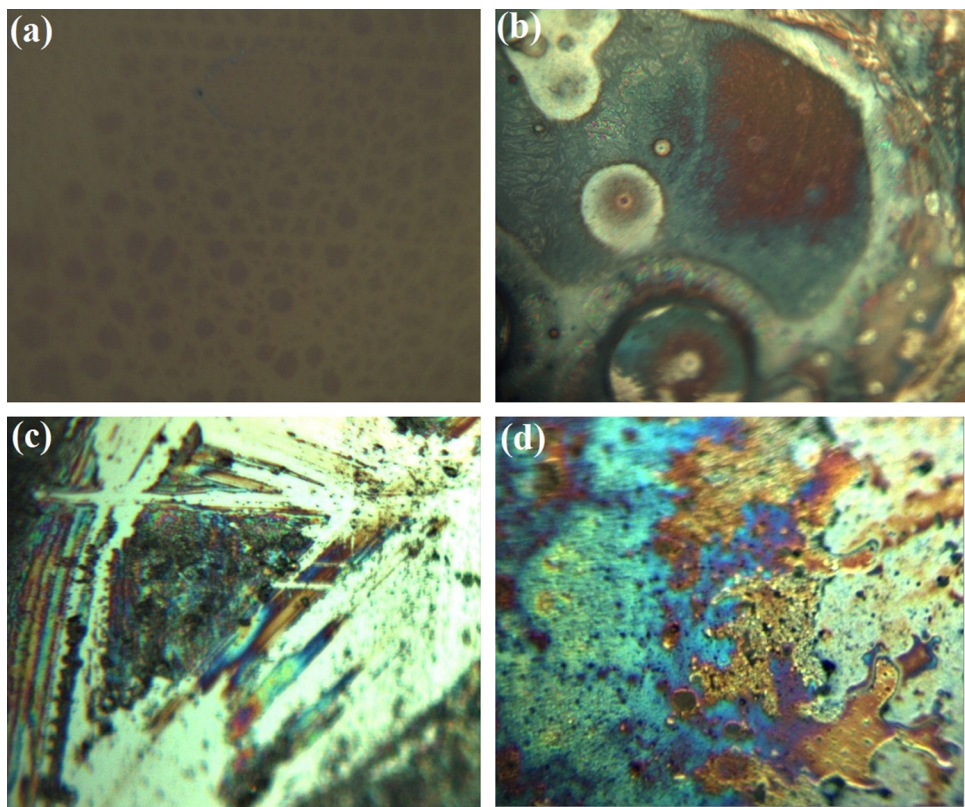


**Fig. 10.** A collection of texture studies optical micrograph of (a) crystals phase porous texture obtained at temperature 90.5 °C, (b) smectic G (Sm G) phase droplet texture appeared at temperature 94 °C, (c) a free standing film of nematic (N) phase pattern is obtained at 97 °C, and (d) twist nematic (TN) oily droplet pattern is obtained at 100 °C.

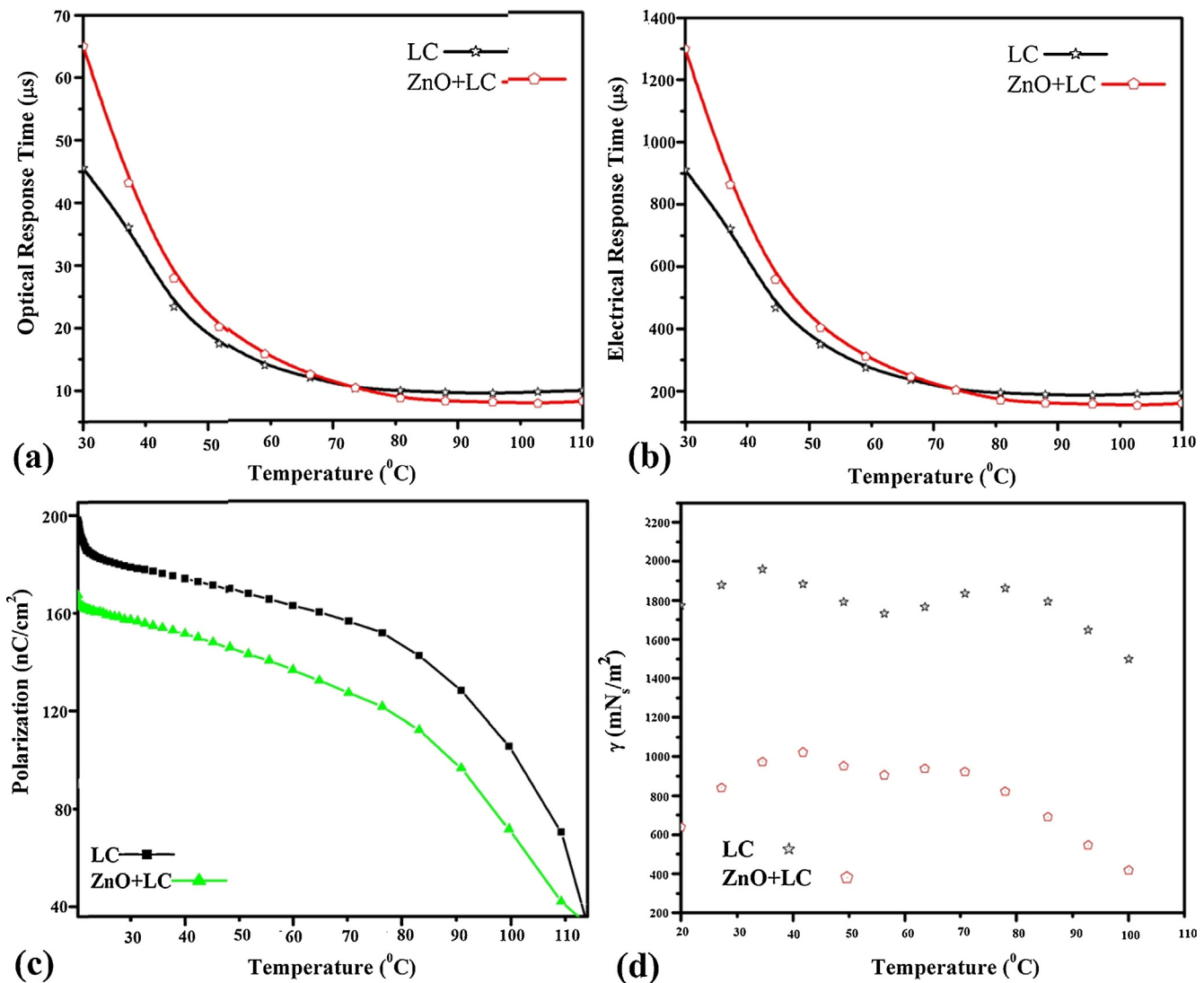


**Fig. 11.** Temperature dependence (a) optical response time, (b) electrical response time, (c) spontaneous polarization ( $P_s$ ), and (d) rotational viscosity ( $\gamma$ ) corresponding to pure liquid crystals and ZnO nanostructures dispersed liquid crystalline material.

The value of temperature dependence spontaneous polarization ( $P_s$ ) of the liquid crystals normally follows a power law which is given by:

$$P_s = P_0(T_c - T)^\gamma \quad (6)$$

where  $P_0$  is constant,  $T_c$  is the Sm G-N phase transition temperature and  $T$  is the temperature at which the measurements are made. Eq. (6) relies on there being a second-order Sm G-N phase transition. In this case mean field theory predicts that should be 0.5. However, detailed investigations of various materials show that the value of this exponent is generally less than this. Interestingly enough, we found that the spontaneous polarization is  $161 \text{ nC cm}^{-2}$  corresponding to ZnO nanomaterials dispersed HBLG (sample containing 33% of HBLG), which is smaller than that of pure HBLG ( $195 \text{ nC cm}^{-2}$ ). Its temperature profile is shown in Fig. 11c. This information provided that the phase separation is complete. This compares reasonably well with the calculated value and implies that incomplete phase separation occurred in the hydrogen bond matrix.

The size of the nano-sphere is sufficiently large to maintain ferroelectric ground state. Thus the multiferroic nanomaterials have finite ferroelectric dipole moments that should interact with the

dipole moments of LC molecules. The electric field exerted by the nanomaterials has the standard dipolar form. We assume the diameter of a nano-sphere is quite large and the average HBLG molecular concentration  $10^{27} \text{ mmol}$ . We investigated that the large electric field interacts with the dipole moment to the surrounding LC molecules. Due to dipole-dipole interaction between the nanomaterials and HBLG molecules the contribution of dipole moment along the transverse direction decreases. This reduces the value of spontaneous polarization in the ZnO embedded HBLG cell which is a measure of transverse dipole moments.

The rotational viscosity is one of the important parameters of the HBLG system that influence response time in Sm G phase. In the present study rotational viscosity has been evaluated by dielectric and electro-optical data as obtained from Eq. (2) and two samples. The temperature dependence of dielectric and electro-optical rotational viscosities are the same, but the absolute values are different from each other by a factor of less than 2 (shown in Fig. 11d). Earlier work reported this difference in dielectric and electro-optical rotational viscosity values for different LCs [64,65]. The reason is that polarization reversal measurement is a large signal method requiring full switching of the hydrogen bonded benzoic acid LC. Therefore, the rotational viscosity curves depend upon the

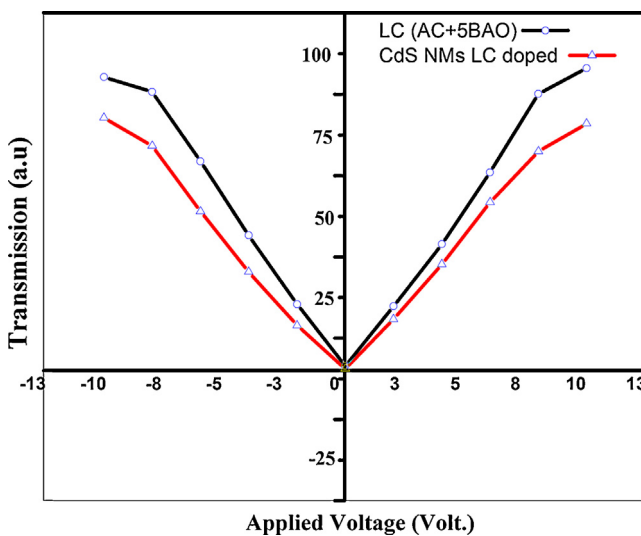


**Fig. 12.** Electro-optical transmittance vs. voltage characteristics of 'V-shape' switching for pure liquid crystals and ZnO doped liquid crystal cell at 35 °C.

spontaneous polarization and thickness of the cell. In the present case, both the spontaneous polarization and cell thickness were small. It can be seen from Fig. 10d that the magnitude of rotational viscosity starts increasing with temperature very slowly from 10 °C below the Sm G–N transition temperature and decreases after showing a hump near the Sm G–N transition temperature.

The light transmittance of pure LC and ZnO nanomaterials dispersed LC modules were measured as a function of the applied voltage at 20 Hz, as shown in Fig. 12. Threshold less, hysteresis-free 'V' shape switching is observed for both the occasions at temperature 35 °C. The voltage required for switching between two electrode system is almost half of the doped cell revealing the enhanced sensitivity of the LC molecules to the applied electric field in the doped system. However, we believe that a cell of thickness less than the pitch of HBLG modules could have given a perfect surface-stabilized state and hence better switching. Applying a square wave voltage of 40 V and 20 Hz, we measured the contrast ratio (maximum transmission/minimum transmission) which

turned out to be the same (0.5) for both the pure LC and doped LC cells.

### 3.7. Dielectric properties by impedance analyzer spectroscopy

Subsequently, we investigated that the excellent behavior dielectric property changes in frequency for pure HBLG and ZnO nanostructures dispersed liquid crystal corresponding to Fig. 13. The value of dielectric constant is extremely high for ZnO nano-sphere is 5.8, with the increase of frequency the all values decreases. Single hump is identified for pure ZnO (indicated by arrow), while two distinct humps are appeared for both pure LC and ZnO nano-structures embedded LC, as shown in Fig. 13a. Hence, Fig. 13b explores the investigation of frequency dispersion dielectric loss. One step behavior of single relaxation peak appeared due to ZnO nanostrucres, while two step behaviors of double relaxation peaks appeared corresponding to the introduction of LC itself and ZnO-nanostructure-LC complex. So a high frequency relaxation phenomenon is observed in the system that also confirmed by dielectric constant variation. Such relaxation may be occurring due to the reorientation of bound charges in the system or its rotational degrees of freedom (DOF).

### 3.8. DC Conductance (I-V characteristics)

In order to study the of I–V response characteristics of ZnO nano-sphere, Liquid crystal, and ZnO nano-sphere blended HBLG illustrated in Fig. 14. Then, forward bias was applied to the circuit while close cycle cryostat systems were used. Generally, current induced were increased due to increases of voltage. Threshold voltage started at 5 V, to transit the charge carrier from the valence band to the conduction band depicted I–V characteristics. Current increases very rapidly corresponding to ZnO nanomaterials. However, the LC materials, respond quite differently and interestingly from doped ZnO nanomaterials. Threshold voltage started almost same like others and the bias field at 9 V little current drops down and again increase similar fashion, while nanomaterials blended LC current sharply falls at 11 V and afterwards increases linear symmetrical fashion with respect to the polarity of the applied voltage. Interestingly, these switches after reaching the peak current i.e. Fall sharply as depicted due to conductor to insulator transition

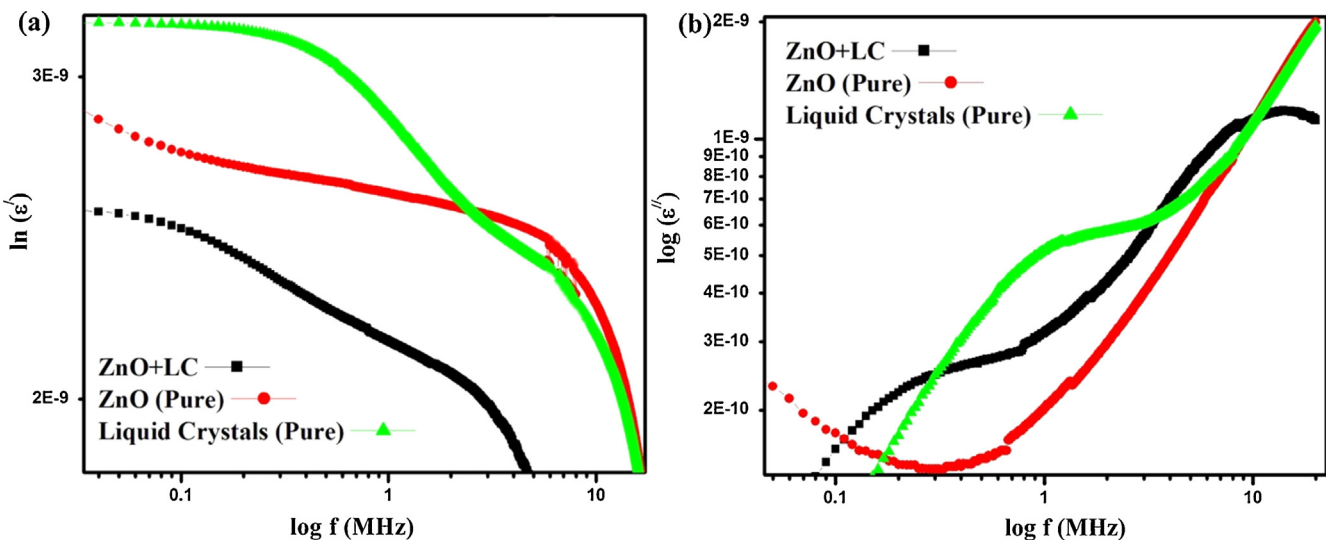


**Fig. 13.** Frequency dispersion dielectric response characteristics of (a) dielectric constant ( $\epsilon'$ ) and (b) dielectric loss ( $\epsilon''$ ), investigation corresponding to pure ZnO nano-sphere and liquid crystal and ZnO embedded liquid crystal.

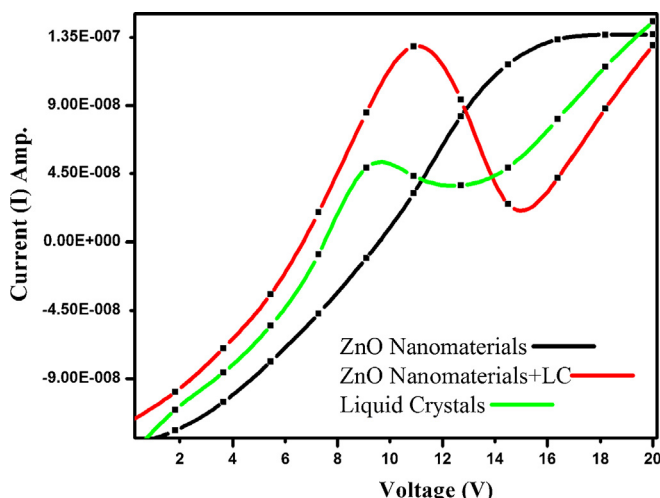


**Fig. 14.** Variation of DC current ( $I$ ) vs. DC voltage ( $V$ ) response characteristics of pure ZnO nanomaterials and Liquid crystals, and ZnO nanomaterials dispersed liquid crystal.

and again conducting behavior of new types of hybrid LC complex nanomaterials. Thus the carrier concentration becomes higher and increasing the conductance.

#### **4. Conclusions**

In summary, we have successfully performed a novel, one-step bench-top synthesis and observed the growth dynamics of ZnO nano-wire to nano-tetrapod and nano-sphere. New superior properties are emerged only when we dispersing nanomaterials into liquid crystal. The special chemical structure can lead to the formation of new twist nematic phase investigated by polarizing optical microscopy. The obtained results suggest that we smoothly dispersed ZnO nanostructures into HBLC. Thus it may conclude that, NDLC is recently found to have a significant influence on the nucleation and growth of many functional nanocrystals, providing a fundamental approach to modify the crystallographic phase, size, morphology, and electronic configuration of nanomaterials. In this article, ZnO nanostructure dispersed liquid crystal offers a significant property of electro-optical switching, ensuring a better bright-field droplet having marble patterns of smectic G phase, nematic and twist nematic phase obtained at specific transition temperature. Notably, the transition temperature at which the twist nematic phase occurs is close to the isotropic temperature, which is a most remarkable signature in NDLC technology. A strong local electric field is produced due to the large dipole moment of the ZnO materials which induces a dipole moment to the neighbor HBLC molecules and reinforces the polarization realignment under electric fields. Charge transfer between LC molecules and ZnO structures weakens the interlayer and intermolecular interaction in the host hydrogen bonded benzoic acid liquid crystals. This in turn reduces the rotational viscosity and response time in the doped cell with smooth distribution, leading to promising applications in smart LCD technology of high contrast ratio.

### **Acknowledgements**

This work was financially supported by the National Natural Science Foundation of China (Project grant No. 61405148) and start-up of Wuhan University, China. Dr. Kaushik Pal is grateful to the above financial support for his postdoctoral study.

## References

- [1] B.O. Regan, M. Graetzel, *Nature* 353 (1991) 737.

[2] M.K. Nazeeruddin, A. Kay, I. Rodicio, R. Humphry-Baker, E. Mueller, P. Liska, N. Vlachopoulos, M. Graetzel, *J. Am. Chem. Soc.* 115 (1993) 6382.

[3] V. Thavasi, R. Jose, S. Ramakrishna, *Mater. Sci. Eng.* 63 (2008) 81.

[4] S.A. Haque, S. Koops, N. Tokmoldin, J.R. Durrant, J. Huang, D.D.C. Bradley, E. Palomares, *Adv. Mater.* 19 (2007) 683.

[5] R. Cinnsealach, G. Boschloo, S.N. Rao, D. Fitzmaurice, *Sol. Energy Mater. Sol. Cells* 55 (1998) 215.

[6] C.G. Granqvist, *Sol. Energy Mater. Sol. Cells* 60 (2000) 201.

[7] M.S. Arnold, P. Avouris, Z.W. Pan, Z.L. Wang, *J. Phys. Chem. B* 107 (2003) 659.

[8] M. Law, H. Kind, B. Messer, F. Kim, P. Yang, *Angew. Chem. Int. Ed. Engl.* 41 (2002) 2405.

[9] Y. Xia, P. Yang, Y. Sun, Y. Wu, B. Mayers, B. Gates, Y. Yin, F. Kim, H. Yan, *Adv. Mater.* 15 (2003) 353.

[10] J. Hu, T.W. Odom, C.M. Liber, *Acc. Chem. Res.* 32 (1999) 435.

[11] F.H. Teherani, C.W. Litton, *Proc. SPIE* 6474 (2007) 647402.

[12] Z.L. Wang, J. Nanosci. Nanotechnol. 8 (2008) 27.

[13] P. Yeh, C. Gu, *Optics of Liquid Crystal Displays*, 2nd ed., John Wiley & Sons, Inc., New York, 2009.

[14] P.G. eGennes, J. Prost, *The Physics of Liquid Crystals*, Clarendon, Oxford, UK, 1995.

[15] G.C. Pimentel, A.L. McClellan, *Annu. Rev. Phys. Chem.* 22 (1971) 347.

[16] T. Elsaesser, H.J. Bakker, *Ultrafast Hydrogen Bonding Dynamics and Proton Transfer. Processes in the Condensed Phase*, vol. 155, Kluwer, Dordrecht, 2002.

[17] L.J. Yu, *Liq. Cryst.* 14 (1993) 1303.

[18] U. Kumar, J.M.J. Frechet, T. Kato, S. Ujile, K. Itmura, *Angew. Chem. Int. Ed. Engl.* 31 (1992) 1531.

[19] V.A. Mallia, M. George, S. Das, *Chem. Mater.* 11 (1999) 207.

[20] J. Ruokolainen, R. Makinen, M. Torkkeli, T. Makela, R. Serimaa, G. Ten Brinke, O. Ikkala, *Science* 280 (1998) 557.

[21] A. Ghanem, C. Noel, *Mol. Cryst. Liq. Cryst. B* 150 (1987) 447.

[22] E. Benedetti, F. Galleschi, E. Chiellini, G. Galli, *J. Polym. Sci. B* 27 (1989) 25.

[23] N.A. Clark, S.T. Lagerwall, *Appl. Phys. Lett.* 36 (1980) 899.

[24] K. Pal, U.N. Maiti, T.P. Majumder, S.C. Debata, S. Ghosh, S.K. Roy, N. Bennis, J.M. Otón, *Nanotechnology* 24 (2013) 125702.

[25] J.W. Goodby, R. Blinc, N.A. Clark, S.T. Lagerwall, S.A. Osipov, S.A. Pinkin, T. Sakurai, Y. Yoshino, B. Zeks, *Ferroelectric Liquid Crystals: Principles, Properties and Applications*, Gorden and Breach, Philadelphia, 1991.

[26] N.A. Clark, S.T. Lagerwall, *Appl. Phys. Lett.* 36 (1980) 899.

[27] A. Fukuda, H. Takezoe, *Structures and Properties of Liquid Crystals*, Corona, Tokyo, 1990.

[28] M.P. Petrov, L.V. Tsonev, *Liq. Cryst.* 21 (1996) 543.

[29] (a) G.W. Gray, B. Jones, *J. Chem. Soc.* (1954) 1467;  
(b) G.W. Gray, *Molecular Structure and Properties of Liquid Crystals*, Academic Press, London, 1962, pp. 163.

[30] H. Kelker, R. Hatz, *Handbook of Liquid Crystals*, VerlagChemie, Weinheim, Germany, 1980.

[31] J. Yu, *Liq. Cryst.* 14 (1993) 1303.

[32] T. Kato, J.M.J. Frechet, *J. Am. Chem. Soc.* 111 (1989) 8533.

[33] T. Kato, H. Kihara, T. Uryu, S. Ujiie, K. Iimura, J.M.J. Frechet, U. Kumar, *Ferroelectronics* 148 (1993) 161.

[34] T. Kato, T. Uryu, F. Kaneuchi, C. Jin, J.M.J. Frechet, *Liq. Cryst.* 14 (1993) 1311.

[35] T. Kato, J.M.J. Frechet, *Macromolecules* 22 (1989) 3818.

[36] U. Kumar, T. Kato, J.M.J. Frechet, *J. Am. Chem. Soc.* 114 (1992) 6630.

[37] H. Kihara, T. Kato, T.S. Ujiie, U.K.umar, J.M.J. Frechet, D.W. Bruce, D.J. Price, *Liq. Cryst.* 21 (1996) 25.

[38] I. Matulkova, I. Nemec, K. Teubner, P. Nemec, Z. Micka, *J. Mol. Struct.* 873 (2008) 46.

[39] B.H. Boo, J.K. Lee, E.C. Lim, *J. Mol. Struct.* 892 (2008) 110.

[40] H. Tanak, F. Ersahin, Y. Koysal, E. Agar, S. Isik, M. Yavuz, *J. Mol. Model.* 15 (2009) 1281.

[41] M. Kurt, T.R. Sertbakan, M. Ozdur, *Spectrochim. Acta A* 70 (2008) 664.

[42] F.F. Jian, P.S. Zhao, Z.S. Bai, L. Zhang, *Struct. Chem.* 16 (2005) 635.

[43] F.F. Jian, P.S. Zhao, Y.X. Hou, *Struct. Chem.* 16 (2005) 361.

[44] Y.X. Sun, Q.L. Hao, W.X. Wei, Z.X. Yu, L.D. Lu, X.J. Wang, *Mol. Struct. Theochem.* 904 (2009) 74.

[45] Y.X. Sun, Q.L. Hao, Z.X. Yu, W.X. Wei, L.D. Lu, X. Wang, *Mol. Phys.* 107 (2009) 223.

[46] P. Bladon, A.C. Griffin, *Macromolecules* 26 (1993) 6604.

[47] C. He, A.M. Donald, A.C. Griffin, T. Waigh, A.H. Windle, *J. Polym. Sci. B: Polym. Phys.* 36 (1998) 1617.

[48] L.C. Chien, M.N. Boyden, A.J. Walz, I.G. Shenouda, C.M. Citano, *Mol. Cryst. Liq. Cryst.* 317 (1998) 273.

[49] P. Nayek, S. Ghosh, S. Karan, T.P. Majumder, S.K. Roy, *Appl. Phys. Lett.* 93 (2008) 112905.

[50] S. Ghosh, P. Nayek, S.K. Roy, R. Gangopadhyay, M.R. Molla, R. Dabrowski, *Appl. Phys. Lett.* 96 (2010) 073101.

[51] M.J. Frisch, G.W. Trucks, H.B. Schlegel, G.E. Scuseria, M.A. Robb, J.R. Cheeseman, J.A. Montgomery Jr., T. Vreven, K.N. Kudin, J.C. Burant, J.M. Millam, S.S. Iyengar, J. Tomasi, V. Barone, B. Mennucci, M. Cossi, G. Scalmani, N. Rega, G.A. Petersson, H. Nakatsuji, M. Hada, M. Ehara, K. Toyota, R. Fukuda, J. Hasegawa, M. Ishida, T. Nakajima, Y. Honda, O. Kitao, H. Nakai, M. Klene, X. Li, J.E. Knox, H.P. Hratchian, J.B. Cross, C. Adamo, J. Jaramillo, R. Gomperts, R.E. Stratmann, O. Yazayev, A.J. Austin, R. Cammi, C. Pomelli, J.W. Ochterski, P.Y.

- Ayala, K. Morokuma, G.A. Voth, P. Salvador, J.J. Dannenberg, V.G. Zakrzewski, S. Dapprich, A.D. Daniels, M.C. Strain, O. Farkas, D.K. Malick, A.D. Rabuck, K. Raghavachari, J.B. Foresman, J.V. Ortiz, Q. Cui, A.G. Baboul, S. Clifford, J. Cioslowski, B.B. Stefanov, G. Liu, A. Liashenko, P. Piskorz, I. Komaromi, R.L. Martin, D.J. Fox, T. Keith, M.A. Al-Laham, C.Y. Peng, A. Nanayakkara, M. Challacombe, P.M.W. Gill, B. Johnson, W. Chen, M.W. Wong, C. Gonzalez, J.A. Pople, Gaussian 03, Revision B.01, Gaussian, Inc., Pittsburgh, PA, New York, 2003.
- [52] A.D. Becke, Phys. Rev. A 38 (1988) 3098.
- [53] C. Lee, W. Yang, R.G. Parr, Phys. Rev. B 37 (1988) 785.
- [54] A.D. Becke, J. Chem. Phys. 98 (1993) 5648.
- [55] P. Hobza, R. Zahradník, Intermolecular Complexes, Elsevier, Amsterdam, 1988.
- [56] F.B. Van Duijneveldt, J.G.C.M. Van Duijneveldt-Van de Rijdt, J.H. Van Lenthe, Chem. Rev. 94 (1994) 1873.
- [57] E.D. Glendening, A.E. Reed, J.E. Carpenter, F. Weinhold, NBO Version 3.1, TCI, University of Wisconsin, Madison, 1998.
- [58] J. Chocholousova, V. Spirko, P. Hobza, Phys. Chem. Chem. Phys. 6 (2004) 37.
- [59] S. Osaki, S. Uemura, Y. Ishida, J. Polym. Sci. 12 (1974) 1727.
- [60] S. Murakami, H. Naito, Jpn. J. Appl. Phys. 36 (1997) 2222.
- [61] K. Pal, U.N. Maiti, T.P. Majumder, S.C. Debnath, J. Appl. Surf. Sci. 258 (2011) 163.
- [62] K. Pal, T.P. Majumder, S. Ghosh, S.K. Roy, J. Mol. Struct. 1041 (2013) 16.
- [63] K. Pal, U.N. Maiti, T.P. Majumder, S.C. Debnath, J. Mol. Struct. 1035 (2013) 76.
- [64] M. Zennyoji, J. Yokoyama, Y. Takanishi, K. Ishikawa, H. Takezoe, K. Itoh, Jpn. J. Appl. Phys. 37 (1998) 6071.
- [65] S.T. Lagerwall, Ferroelectric and Antiferroelectric Liquid Crystals, Wiley-VCH, Weinheim, 1999, pp. 200.